DOI: 10.3901/CJME.2014.01.041, available online at www.springerlink.com; www.cjmenet.com; www.cjmenet.com.cn

Numerical Analysis of Rolling-sliding Contact with the Frictional Heat in Rail

LI Wei, WEN Zefeng*, JIN Xuesong, and WU Lei

State Key Laboratory of Traction Power, Southwest Jiaotong University, Chengdu 610031, China

Received January 12, 2013; revised August 19, 2013; accepted November 5, 2013

Abstract: Thermal damage caused by frictional heat of rolling-sliding contact is one of the most important failure forms of wheel and rail. Many studies of wheel-rail frictional heating have been devoted to the temperature field, but few literatures focus on wheel-rail thermal stress caused by frictional heating. However, the wheel-rail creepage is one of important influencing factors of the thermal stress. In this paper, a thermo-mechanical coupling model of wheel-rail rolling-sliding contact is developed using thermo-elasto-plastic finite element method. The effect of the wheel-rail elastic creepage on the distribution of heat flux is investigated using the numerical model in which the temperature-dependent material properties are taken into consideration. The moving wheel-rail contact force and the frictional heating are used to simulate the wheel rolling on the rail. The effect of the creepage on the temperature rise, thermal strain, residual stress and residual strain under wheel-rail sliding-rolling contact are investigated. The investigation results show that the thermally affected zone exists mainly in a very thin layer of material near the rail contact surface during the rolling-sliding contact. Both the temperature and thermal strain of rail increase with increasing creepage. The residual stresses induced by the frictional heat in the surface layer of rail appear to be tensile. When the creepage is large, the frictional heat has a significant influence on the residual stresses and residual strains of rail. This paper develops a thermo-mechanical coupling model of wheel-rail rolling-sliding contact, and the obtained results can help to understand the mechanism of wheel/rail frictional thermal fatigue.

Keywords: wheel-rail rolling-sliding contact, frictional heating, creepage, residual stress/strain, thermo-elasto-plastic finite element method

1 Introduction

In railway engineering, the thermal damage, as a difficult topic of wheel-rail system research, is one form of wheel-rail rolling contact fatigue failure in the high speed and heavy haul operation[1–2]. The frictional heat at the wheel-rail contact area is generated by the relative slip between the wheel-rail contact surfaces. The thermal stress induced by the frictional heat can impel the initiation and propagation of cracks in wheel and rail. To reveal the mechanism of the thermal damage and reduce the thermal damage phenomenon, it is necessary to study the temperature and stress/strain distributions of wheel and rail in various operating situations.

Many studies have been devoted to the temperature field during the wheel-rail rolling/sliding contact [3–8]. However, few literatures on wheel-rail thermal stress due to frictional heating are reported. ERTZ, et al[9], proposed an analytical solution for the surface temperature rise and thermal stress generation during the rolling contact of wheel subject to sliding friction. They pointed out that the thermal stresses greatly affect the shakedown limit in wheel/rail contact. FISCHER, et al[10], established the thermo-elastic plane strain finite element model to analyze the stress state due to the wheel-rail sliding friction. However, the effect of the mechanical load or the wheel-rail normal contact load and tangential load was not considered in the model. KULKARNI, et al[11], employed the finite element package ABAQUS to calculate the temperature and stress-strain distributions of rail under the wheel-rail rolling/sliding contact. In the thermo-mechanical coupling model, material properties were assumed to be temperature independent. WIDIYARTA, et al[12], presented the computer simulation of wear and crack initiation based on the ratcheting failure with thermal effect. They found that the frictional heating effects increase the rate of damage accumulation by ratcheting, leading to increased wear and rolling contact fatigue. WU, et al[13], used a finite element method to analyze the wheel-rail fiction thermal elastic-plastic deformation and residual stress during different wheels sliding over rail. MARSYM, et al[14], numerically calculated the temperature distribution between wheel and rail in the flange contact area. The proposed algorithm makes it possible to detect the lubrication type or lubricant additive in the contact. WEN, et al[15], utilized the finite element analysis to study the elastic-plastic deformation

* Corresponding author. E-mail: zefengwen@126.com

This project is supported by National Natural Science Foundation of China (Grant Nos. 51175438, U1134202), National Science and Technology Support Program of China (Grant No. 2009BAG12A01), and Program for New Century Excellent Talents in University of China (Grant No. NCET-08-0824)

and residual stress and strain under the non-steady state rolling contact between wheel and rail. The obtained numerical results show that the creepage or stick-slip condition greatly influences the residual stresses and strains. However, the effect of temperature was neglected.

The aim of the present paper is to investigate the effect of the creepage on the temperature rise, residual stress and residual strain under wheel-rail sliding/rolling contact. A thermo-mechanical coupling elastic-plastic plane strain finite element model for wheel-rail contact is developed by using the finite element code ABAQUS. The heat-convection between the rail and surrounding air and temperature-dependent material properties are taken into consideration.

2 Numerical Modeling

2.1 Model of wheel-rail contact

When a wheel and a rail get into contact under the action of the static wheel load, the contact area and the pressure distribution are usually determined by using the Hertz theory. The normal pressure distribution is [16]

$$p(x,z)=p_0\sqrt{1-\frac{x^2}{a^2}-\frac{z^2}{b^2}}, \tag{1}$$

where x and z are the local coordinates in the longitudinal and lateral directions, respectively. $p_0(=3P/\pi ab)$ is the maximum contact pressure, P is the total normal contact force. a and b are the semi-axes of the contact ellipse. In railway engineering, the wheel-rail contact patch becomes a slim elliptical shape in the lateral direction after a long-term wear, as shown in Fig. 1.

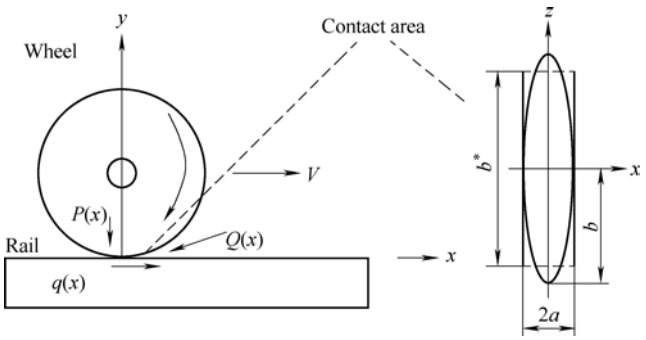

Fig. 1. Wheel-rail in sliding contact and slim contact area

The three-dimensional rolling contact problem is simplified to be a two-dimensional problem to determine the stress and temperature fields in wheel-rail contact in this paper. The two-dimensional contact model (2D model) is time saving. In the 2D model, the normal pressure at any point of the contact ellipse of a wheel rolling on the rail is

$$p(x)=p_0\sqrt{1-\frac{x^2}{a^2}}, \tag{2}$$

where the maximum pressure can be expressed as

$$p_0=\frac{2P}{\pi ab^*}, \tag{3}$$

$b^*(=4b/3)$ is the equivalent length of the contact patch in the lateral direction. The equivalent concept is based on the condition that the maximum Hertzian pressures are identical in the three-dimensional and the two-dimensional cases. In addition, the contact lengths in the longitudinal direction are identical in the two cases.

To consider the partial slip condition, the contact area is divided into slip and stick zones, as shown in Fig. 2. In the stick zone, the materials of two contact bodies have identical micro-slip velocities. In the slip zone, the tangential force is proportional to the normal pressure. Carter derived the tangential force distribution for the two-dimensional partial slip elastic rolling contact. The mathematical expressions for the tangential force distribution in the slip and stick zones of the contact area, $q(x)$, are as follows [17]

$$q(x)=\begin{cases}q'(x), & -a\leqslant x\leqslant -c+d_s,\\ q'(x)+q''(x), & -c+d_s\leqslant x\leqslant a,\end{cases} \tag{4}$$

where

$$q'(x)=fp(x), \tag{5}$$

$$q''(x)=-\frac{c}{a}fp_0\left\{1-\left(\frac{x-d_s}{c}\right)^2\right\}^{1/2}, \tag{6}$$

where f is the friction coefficient. c represents the half width of the stick area, and $d_s=a-c$ is the distance between the centers of the slip and stick region. A graphic illustration of Eq. (4) is shown in Fig. 2.

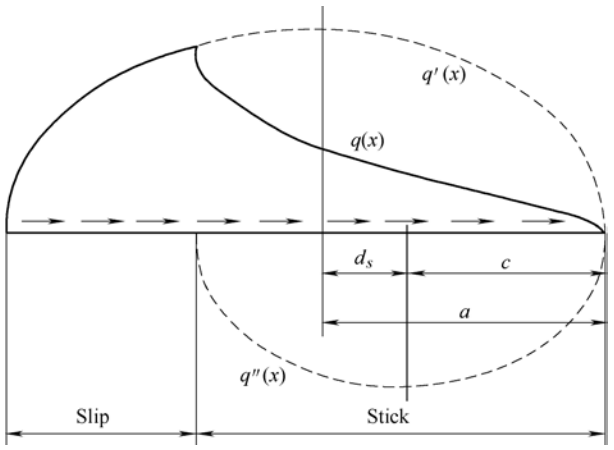

Fig. 2. Tangential force distribution for line rolling contact

If the two contact elastic bodies with the same physical properties can be modeled as two half spaces contacting

each other, the tangent traction has no effect on the normal pressure distribution, the geometry shape and size of the contact patch[16]. In the paper, the physical properties of a wheel and a rail are assumed to be the same. And compared to the geometry characteristic size of the wheel and the rail and curvature radius near the wheel-rail contact patch, the size of the contact patch appears to be very small. Therefore, in the present study it is assumed that the effect of tangent traction on the distribution of normal pressure is neglected in the wheel-rail contact model.

In the paper, the irregularities of wheel and rail in the straight track are not considered and the wheel-rail contact force is constant. The numerical analysis of non-steady state partial slip wheel-rail rolling contact can be found in Ref. [15]. The effect of rail corrugation on the wheel-rail thermal contact pressure and temperature distributions during wheel braking was investigated by using the finite element method in Ref. [19].

In Eq. (4), the stick zone size is determined by the contact load using the following equation

$$\frac{c}{a}=\left(1-\frac{Q}{fP}\right)^{1/2}, \tag{7}$$

where Q denotes the total tangential force.

When a wheelset is moving on a track, the interface of wheel/rail contact patch has a relative slip caused by the wheel/rail rigid movement, their local elastic deformation and the structure elastic deformation of the wheelset/track. The total slip of wheel/rail contact patch consists of rigid slip and elastic slip. And the rigid and elastic relative slips are represented by the rigid and elastic creepages, respectively. The rigid creepage is the ratio of the difference in velocity of the two surfaces over the mean velocity. And the elastic creepage is the rate of the change of the relative tangential elastic deformation of a pair of the contact points. The detailed description of the creepages can be found in Ref. [20].

The rigid creepage, ξ, can be determined by using Carter's equation [16]

$$\xi=-\frac{fa}{R}\left(1-\sqrt{1-\frac{Q}{fP}}\right)=-2fp_0E^*\left(1-\sqrt{1-\frac{Q}{fP}}\right), \tag{8}$$

where R is the nominal rolling radius of the wheel and E^* is the elastic contact modulus which is determined using the following equation

$$E^*=\frac{1-\upsilon_1^2}{E_1}+\frac{1-\upsilon_2^2}{E_2}, \tag{9}$$

where E_1 and E_2 are the Young's module of wheel and rail materials, respectively, and υ_1 and υ_2 are the Poisson's ratios of the wheel and rail materials, respectively.

By using the rigid creepage, ξ, Eq. (8) can be rewritten as[20]

$$\frac{Q}{fP}=\begin{cases}-\dfrac{2R}{fa}\xi+\dfrac{1}{4}\left(\dfrac{2R}{fa}\right)^2|\xi|\xi, & \text{when } \dfrac{2R}{fa}|\xi|\leqslant 2,\\ -\text{sgn}(\xi), & \text{when } \dfrac{2R}{fa}|\xi|>2,\end{cases} \tag{10}$$

where ξ=0 represents the pure rolling case. When $|\xi|=fa/R$, the stick area diminishes, corresponding to the full slip case. The partial slip is represented by $0<|\xi|<fa/R$.

The total longitudinal creepage of wheel-rail, w, equals the sum of the rigid creepage ξ and elastic creepage $\partial u/\partial x+(\partial u/\partial t)/v_0$ due to the deformation of wheel-rail. Considering the steady state partial slip in wheel-rail rolling contact, namely $\partial u/\partial t=0$, the sliding equation for a pair of contacting particles in the contact is written as [20]

$$w(x)=\xi-\frac{\partial u}{\partial x}=\xi-\begin{cases}-\dfrac{2fp_0}{aE^*}x, & \text{slip zone},\\ -\dfrac{d_s}{a}\dfrac{2fp_0}{E^*}, & \text{stick zone},\end{cases} \tag{11}$$

where u denotes the tangential elastic deformation difference between a pair of the contacting particles. In the stick zone, w=0.

The thermal flux per unit area and per unit time in the contact area can be given as [3]

$$Q(x)=q(x)w(x)V, \tag{12}$$

where V is the rolling speed of the wheel. It is assumed that the mechanical energy generated by friction in the contact patch is transformed completely into heat. And a heat partition factor, representing the fraction heat flow rate entering the rail, is assumed as constant value 0.5 [4].

2.2 Finite element model

In this study, a fully coupled thermal-stress analysis is employed because the stresses are dependent on the temperature distribution in rolling/sliding contact. The mechanical and thermal solutions are obtained simultaneously in the analysis. The coupled temperature-displacement elements are considered in the modeling. The temperature is calculated using a backward-difference scheme, and the nonlinear equations are solved using Newton's method.

An exact implementation of Newton's method involves a non-symmetric Jacobin matrix as illustrated in the following coupled equations

$$\begin{pmatrix}\boldsymbol{K}_{uu} & \boldsymbol{K}_{uT}\\ \boldsymbol{K}_{Tu} & \boldsymbol{K}_{TT}\end{pmatrix}\begin{pmatrix}\Delta\boldsymbol{U}\\ \Delta\boldsymbol{T}\end{pmatrix}=\begin{pmatrix}\boldsymbol{R}_u\\ \boldsymbol{R}_T\end{pmatrix}, \tag{13}$$

where $\Delta \boldsymbol{U}$ and $\Delta \boldsymbol{T}$ are the corrections to the incremental displacement and temperature, respectively. $\boldsymbol{K}_{ij}$ are sub-matrices of the fully coupled Jacobin matrix, and $\boldsymbol{R}_u$ and $\boldsymbol{R}_T$ are the vectors of the mechanical and thermal residual loads, respectively.

The line contact is assumed to be a plane strain problem. The two-dimensional coupling thermo-mechanical finite element model for rail is developed to investigate the elastic-plastic strain/stress state and the temperature rise in the rail, during a wheel rolling/sliding on it, as shown in Fig. 3. In the numerical model, the rail is modeled by a rectangle with the length of 150 mm and height of 30 mm. The above size of rail model is determined by trial investigation and is large enough to eliminate the end effect. The heat-convection between the rail and its ambient and the temperature-dependent material properties are taken into consideration. The bottom and two ends of the rail are assumed to be insulated and fixed. The frictional heat source generated by wheel-rail rolling/sliding contact is simulated by the flux boundary condition. The normal pressure and the tangent traction obtained by Eqs. (2) and (4) in the contact patch are used as the boundary forces for the FE model. The movement of contact patch is simulated by the moving boundary conditions. The rail mesh consists of 22 500 4-node bilinear coupled temperature-displacement plane strain elements and 22 936 nodes. Because the thermal effects due to friction only exist in the thin layers near the contact surface, fine mesh is used near the contact surface of the rail, as shown in Fig. 3. The size of the smallest element is about 0.4 mm×0.05 mm. A number of steps are utilized to translate the boundary conditions of the contact patch from point A to point B, as shown in Fig. 3. After the contact load and the frictional heat resource reach point B, the load and the frictional heat are decreased gradually in incremental steps. The temperature rise and the stresses approach to the steady state after the contact load and the frictional heat source move the three contact patches. The present numerical analysis considers the length of six contact patches during a wheel rolling/sliding on the rail.

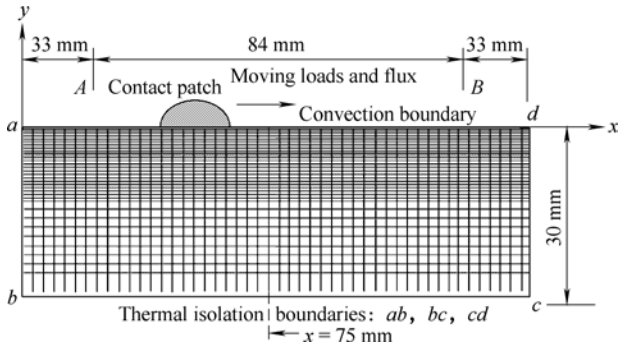

Fig. 3. Finite element mesh model

3 Results and Discussions

In the present numerical analysis, a locomotive wheel with profile of JM1, the axle load W=23 t and rolling radius R=525 mm is selected. The rail is CHN60 of China. According to Hertzian theory, the semi-axis of the contact ellipse in the longitudinal direction is a=7.0 mm and the maximum contact pressure P_0=878 MPa [20]. The density of rail material is 7 790 kg/m^3. The ambient temperature T_0 is 20 °C, and the heat transfer coefficient between the rail surface and the ambient is selected as h=20 W • m^{-2} • K^{-1}. The coefficient of friction between wheel-rail contact is assumed to be 0.3. The rolling speed of the wheel is about 120 km/h. The linear kinematic hardening model is used for plasticity calculation of the rail material. The value of ET/E is assumed to be 0.1. ET is the tangent modulus. In this paper, the influence of wheel-rail frictional temperature rise on the material properties of the rail is taken into account. The temperature-dependent material properties of rail are listed in Table 1 and Table 2[21].

Table 1. Temperature-dependent material properties

Temperature T/°C	Specific heat c_p/(J • kg^{-1} • K^{-1})	Thermal conductivity k/(W • m^{-1} • K^{-1})
0	419.5	59.71
350	629.5	40.88
703	744.5	30.21
710	652.9	30.00
800	657.7	25.00
950	665.2	27.05

Table 2. Temperature-dependent material properties

Temperature T/°C	Young's modulus E/GPa	Poisson's ratio υ	Yield stress S_y/MPa	Coefficient of thermal expansion α/10^{-6} K^{-1}
0	213	0.295	483.0	9.97
24	213	0.295	483.0	9.97
230	201	0.307	485.1	10.82
358	193	0.314	418.8	11.15
452	172	0.320	332.4	11.27
567	102	0.326	151.1	11.31

Fig. 4 shows the distribution of heat flux for the different creepages during the wheel-rail rolling/sliding contact. In Fig. 4, the solid and dotted lines represent the results of the total creepage and rigid creepage, respectively. Fig. 5 presents the temperature difference ratio, which is defined as $(T_{tc}-T_{rc})/T_{tc}$, where T_{tc} is the temperature due to the total creepage considering the elastic creepage and T_{rc} is the one due to the rigid creepage neglecting the elastic creepage in the rail surface. From Figs. 3 and 4, it is noted that the effect of elastic creepage on the heat flux generated by the wheel-rail friction and the temperature rise of rail material is attenuated as the rigid creepage increases. According to Eq. (11), when the rigid creepage value ξ increases, the effect of elastic creepage $\partial u/\partial x$ on the total creepage $w(x)$ becomes weak. And the difference of the thermal flux $Q(x)$ under rigid creepage and total creepage becomes small with increasing ξ, as seen in Fig. 4. The value of temperature rise is dependent on the thermal flux. So the temperature difference ratio $(T_{tc}-T_{rc})/T_{tc}$ is decreasing as the ceepage increases.

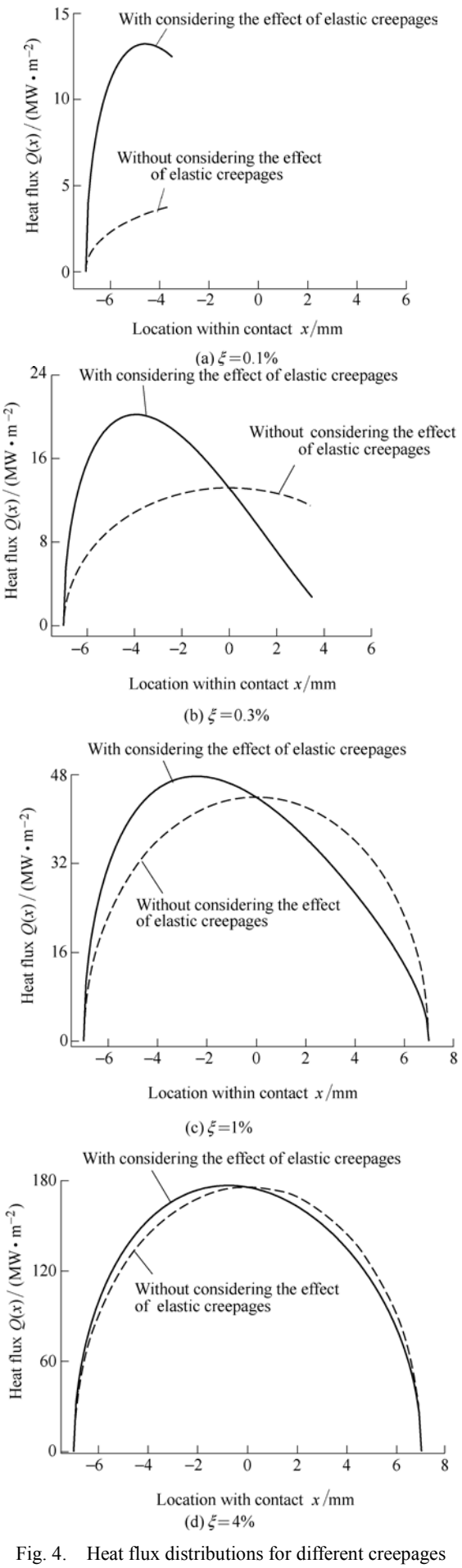

Fig. 4. Heat flux distributions for different creepages

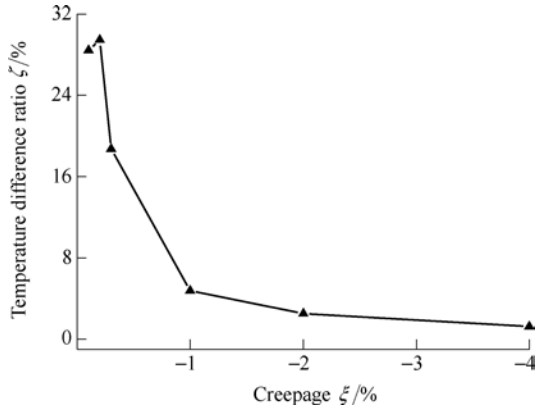

Fig. 5. Variation of temperature difference ratio with creepage

In order to investigate the effect of creepage of wheel/rail contact on the temperature rise, residual stress and residual strain of the rail, five creepages (−0.1%, −0.2%, −0.3%, −2%, and −4%) are considered in the simulations. According to Eq. (8), the critical value of the creepage determined by $\xi=-a \cdot f/r_w$ is about −0.4%. If $|\xi| \geqslant 0.4\%$, a full slip state of wheel-rail contact will happen.

Figs. 6 and 7 show the variations of the temperature and the longitudinal thermal strain (along the x direction) with the vertical depth of the rail for the different creepages, respectively. From Figs. 6 and 7, it is known that the temperature rise and the longitudinal thermal strain in the surface layer of rail increase as the creepage increases and the effect of the creepage on the material temperature and strain of rail surface is significant. Comparing Fig. 6 with Fig. 7, it can be found that the thermal strain of rail material is proportional to the temperature rise. When the creepage increases from −0.3% to −2%, the maximum temperature increases from about 41 °C to about 134 °C, which can induce the appreciable thermal stress in the material of the rail surface. The zone affected by the temperature rise exists in the thin layer of 0.3 mm close to the rail top during the wheel-rail sliding/rolling contact.

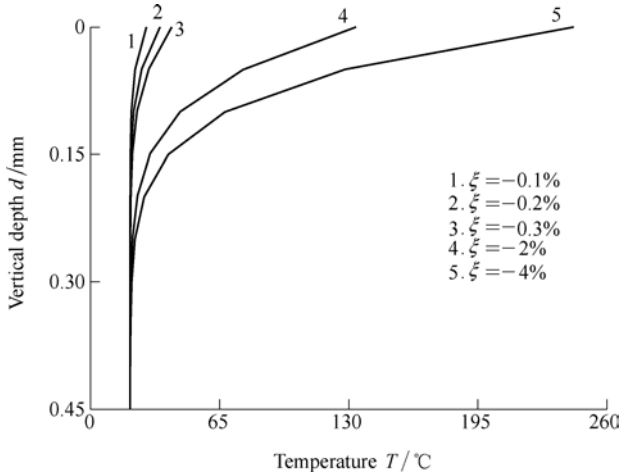

Fig. 6. Variation of temperature with depth for different creepages

Since the zone affected by the temperature rise exists in the thin layer of 0.3 mm close to the rail top, to be

convenient for analysis, the residual stress and residual strain in the depth of about 1 mm from the rail top surface are shown in the following results. All the following results reported are taken from the middle cross section of rail model (i.e., x=75 mm, as shown in Fig. 3) at which the effect of the rail ends is very small. In the present simulation，a single wheel pass is considered. Two cases of the wheel-rail contact are analyzed: case 1 is for the thermo-mechanical coupling simulation, case 2 for the only mechanical loading simulation without considering thermal effect. The results for case 1 and case 2 are shown with the solid lines and the dashed ones in the following figures, respectively.

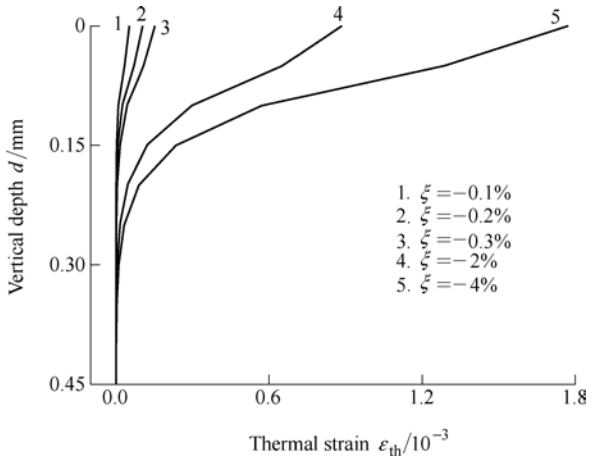

Fig. 7. Variation of thermal strain with depth for different creepages

Fig. 8 illustrates the variation of Von Mises equivalent residual stress $(\sigma_e)_r$ with the depth for different creepages.

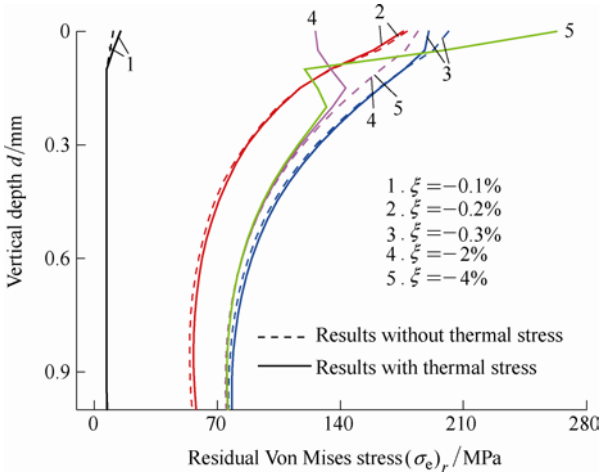

Fig. 8. Variation of residual Von Mises stress with depth for different creepages

Comparing case 1 with case 2, the thermal response for the low creepages (ξ=−0.1%, −0.2%, −0.3%) has little effect on the residual equivalent stress in the surface layer of rail, as shown in Fig. 8. It is because that the fictional heat generated by the sliding for the lower creepages results in the lower temperature rise (as seen in Fig. 6). However, the effect on the residual equivalent stress in the layer of the rail surface becomes large as the creepage increases (ξ=−2%, −4%). The residual equivalent stress for case 2 is larger than that for case 1 when creepages (ξ=−0.2%, −0.3%, −2%) are lower. But when the creepage increases to a certain value (−4%), the residual equivalent stress for case 1 is larger than that for case 2.

The variations of the residual stresses in the x and z directions ($(\sigma_x)_r$ and $(\sigma_z)_r$) with the depth for the different creepages are shown in Figs. 9(a) and 9(b), respectively.

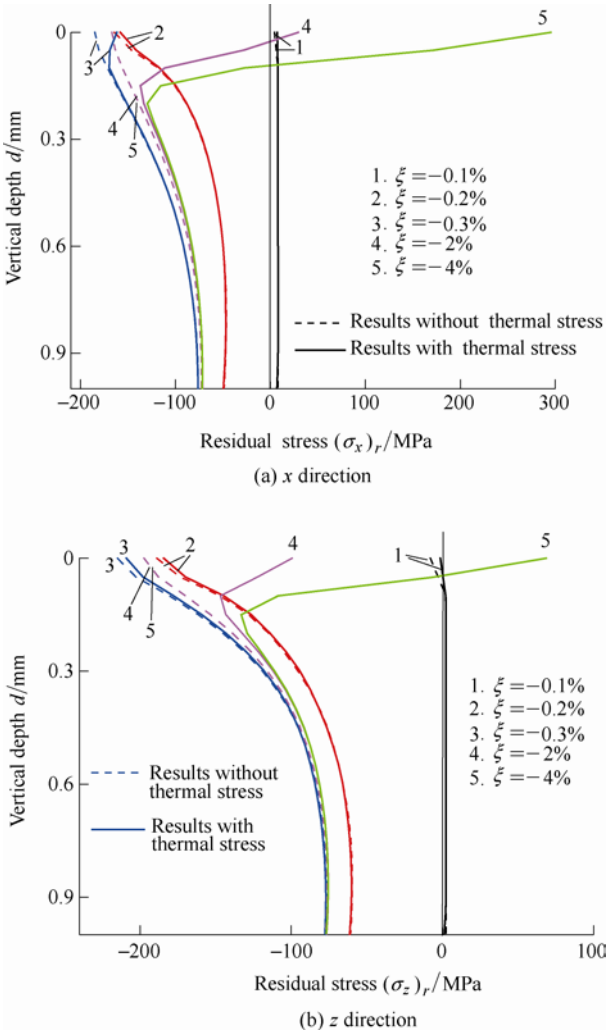

Fig. 9. Variation of residual stress in the x and z directions with depth for different creepages

From Fig. 9, it is seen that the residual stresses in the x and z directions for case 1 appear to be tensile stresses, but those for case 2 appear to be compressive stresses when the creepage increases to a certain value (ξ=−4%). The reason is that the temperature of the surface layer material of rail decreases more steeply than that of the subsurface layer material. And the temperature of the surface layer material becomes higher than that of the subsurface layer material. After cooling shrinkage, the surface material of the rail is in the tensile state for keeping the continuous material deformation. Therefore, the thermal effect easily causes the surface crack initiation in the wheel-rail contact area. For the lower creepages (ξ=−0.1%, −0.2%, −0.3%), the

thermal loads have little effect on the residual stress distribution. Near the rail surface the residual stress in the x and z directions induced by the mechanical load is compressive. The thermal load caused by the small creepages can reduce the residual compressive stresses generated by the mechanical load. But as the creepage increases ($\xi=-4\%$), the effect of the thermal load becomes more significant and the residual stress in the x and z directions near the rail surface exhibit the tensile stress. The results show that the thermal load in the surface layer of rail caused by the temperature rise can lead to the tensile residual stress, and the wheel load can lead to the compressive residual stress. Therefore, the thermal load is destructive. And it is necessary to avoid the high creepage operation of the vehicles.

Figs. 10(a) and 10(b) illustrate the variations of the residual shear strain $(\gamma_{xy})_r$ and the residual equivalent plastic strain $(\varepsilon_p)_r$ with the depth for the different creepages, respectively.

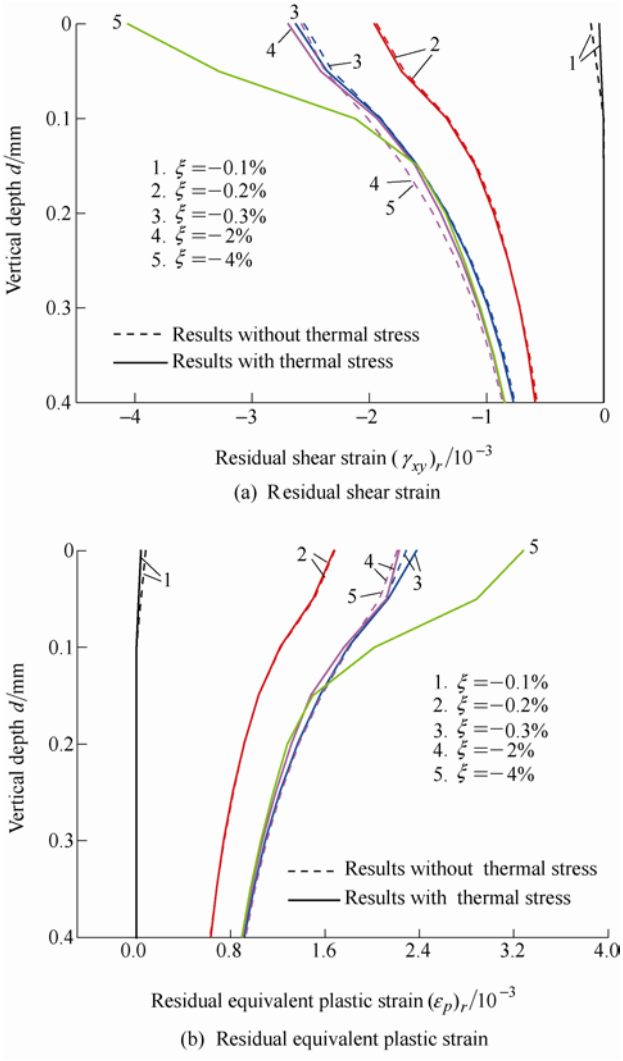

Fig. 10. Variation of residual equivalent plastic strain and residual shear strain with depth for different creepages

From Figs. 10(a) and 10(b), the residual shear strains and the residual equivalent plastic strains for case 1 and case 2 increase with increasing creepage. When the creepages ξ is -0.1%, -0.2%, -0.3%, and -2%, the maximum residual shear strain for case 1 is only about 5% larger than that for case 2. But when the creepage reaches -4%, the maximum residual shear strain and the maximum residual equivalent plastic strain for case 1 are larger than those for case 2 by 57.51% and 48.27%, respectively. It is because when the temperature caused by the wheel-rail friction increases to a certain value, its effect on the material properties (seen in Table 1 and Table 2) is enough to soften the rail surface material. Probably a certain critical value range existing between -2% and -4% can result in the abrupt change of the residual plastic strain. Besides the effect of the thermal load on the residual strain is in about 0.3 mm depth, which corresponds to the affected zone of the temperature rise.

4 Further Discussion

The present study is based on the simplified assumptions which were also used in Refs. [3–9]. First, in the slip zone during wheel-rail rolling-sliding contact, the heat generated at the interface of wheel and rail produces a certain thermal distortion. And the thermal deformation has an effect on the contact area size, the slip zone size and the distributions of normal pressure and tangential tractions which cause the frictional heating[18]. In this paper, the effect of the thermal deformation on the above parameters related to the contact area is neglected and will be investigated in the near future.

The present work is an attempt to couple the wheel-rail contact mechanical load with the thermal load due to wheel-rail frictional heating in the modeling. The contact pressure is assumed to follow the idealized Hertzian distribution and the Carter tangential force distribution is used. Both distributions are based on elastic solutions. A more realistic consideration should include the influences of the plastic deformation, the geometry of the wheel and the rail and dynamics behavior on the contact forces. From Fig. 4, it can be found that when the creepage $|\xi|<0.74\%$, the temperature difference ratio is larger than 10%. And the results obtained (as shown in Figs. 3 and 4) show the effect of the elastic creepage due to the elastic deformation of wheel and rail on the frictional heating should be considered when the creepage $|\xi|<0.74\%$.

Fig. 11 shows the variation of the maximum temperature of rail surface with the total creepage. The maximum temperature of rail material linearly increases as the wheel-rail creepage increases. Because the maximum temperature is below about 40.94 °C when the creepage $|\xi|<0.3\%$, the effect of wheel-rail creepage on the thermal stress is not obvious when the creepage $|\xi|<0.3\%$, as shown in Figs. 8 and 9. When the temperature of rail material is over 600 °C, the thermally induced phase transformation of the material occurs[22]. From Fig. 11, it can be found that the maximum temperature of rail material is only about 245 °C when the creepage $|\xi|=4\%$. However, although temperature-induced martensitic transformation does not

happen under the conditions given in this paper, the temperature rise of rail material cannot be neglected. Temperature rises of about 50 °C would affect stresses in the same magnitude as the mechanical loads do[4]. Actually the wheel-rail frictional temperature rise of above 600 °C may occur in certain extreme circumstances, such as the larger wheel-rail frictional coefficient, heavier wheel loads with the above creepage, and the wheel sliding on the rail during braking and traction[3, 11, 22]. In order to clearly understand the mechanism of wheel/rail frictional thermal fatigue, it is very necessary to investigate some exceptional service conditions in the future work.

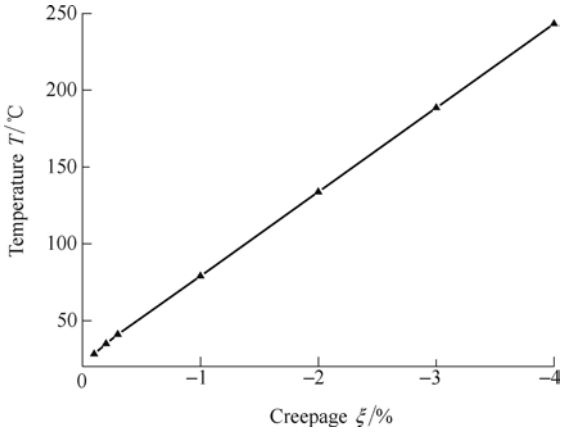

Fig. 11. Maximum temperatures of the rail surface material for different wheel-rail creepages

Although the affected zone of temperature rise exists in the surface layer of the rail with the depth of about 0.3 mm during wheel-rail sliding/rolling contact, the high temperature of rail material which results in thermal plastic deformations occur in a very thin surface layer of about 70 μm depth, as shown in Figs. 8–10. It coincides with the results of Refs. [4] and [23].

To simplify the modeling for the wheel-rail contact with the frictional heating, the wheel rolling over the rail is simulated with the translation of boundary conditions of contact patch across the contact surface in this paper. The heat transfer from the wheel to the rail through the contact patch is neglected. The effect of the heat transfer between the wheel and rail on the temperature rise was investigated in Ref. [5]. The influence of wheel-rail friction coefficient on the frictional heating is not investigated in the paper. However, the high temperature rise due to wheel-rail friction has an influence on the wheel-rail frictional coefficient which is related to many factors, such as the material physical properties, the status of the contact surfaces, the contact load, the environment, etc.

The assumptions of complete energy transformation into heat, no heat loss and the constant heat partition factor during wheel-rail rolling-sliding contact are considered in the modeling. However, the numerical results including the wheel-rail frictional heating depend on the heat partition factor value which determines the heat distribution partitioned into the wheel and rail. Ref. [8] makes an investigation into the effect of the varying of the heat distribution partitioned into the wheel and the rail on the temperature rise in the wheel and the rail.

The contact surfaces of wheel and rail are subjected to high stress and high temperature generated by wheel-rail friction. The high temperatures of the surfaces due to wheel-rail friction occur instantaneously. Therefore, it is difficult to obtain the value of the transient temperature rise of wheel and rail through the experimental investigation. In the paper, the experimental analysis on wheel-rail contact temperature rise is not given. Due to the complication of real wheel-rail contact problem and the limitation of computer ability, the three-dimensional wheel-rail contact problem has to be assumed to a two-dimensional problem. The three-dimensional wheel-rail contact model and the more complicated contact conditions will be investigated in the future study.

5 Conclusions

(1) Based on the thermo-elasto-plastic finite element method, a thermo-mechanical coupling numerical analysis is performed to investigate the states of the strain/stress and the temperature rise of rail during wheel-rail sliding/rolling contact. The results show that the temperature rise and thermal strains in the surface layer of rail increase as the creepage increases.

(2) The residual stresses in thin layer of rail in the circumferential and axial directions induced by the thermal loads appear to be tensile.

(3) The effects of the thermal load on the residual stress and the residual strain are significant for the high creepages and the thermal affected zone exists in the thin layer of rail surface with depth of about 0.3 mm during wheel-rail sliding/rolling contact.

(4) When the creepage reaches a certain critical value, the circumferential and axial residual stresses in the thermo-mechanical case become tensile stresses, while in the mechanical case they appear to be compressive stresses. And the residual stress and the residual strain in the surface layer of rail increase with increasing creepage.

Acknowledgments

The authors are grateful to thank associate professor WANG Hengyu at State Key Laboratory of Traction Power of Southwest Jiaotong University, China, for his kind help in improving the English text of the paper.

References

[1] ZHANG Bin, LU Guanjian, FU Xiuqin, et al. Fai*lure analysis and metallography of damage in railway wheels and tyres*[M]. Beijing: China Railway Publishing House Press, 2002. (in Chinese)

[2] YANG Ke, LU Guanjian, YUAN Longying, et al. *Rail damage metallography*[M]. Beijing: China Railway Publishing House Press, 1992. (in Chinese)

[3] TANVIR M A. Temperature rise due to slip between wheel and

rail-an analytical solution for Herzian contact[J]. *Wear*, 1980, 61(2): 295–308.

[4] KNOTHE K, LIEBELT S. Determination of temperatures for sliding contact with applications for wheel–rail systems[J]. *Wear*, 1995, 189(1–2): 91–99.

[5] GUPTA V, HAHN G T, BASTIAS P C, et al. Calculations of the frictional heating of a locomotive wheel attending rolling plus sliding[J]. *Wear*, 1996, 191(1–2): 237–241.

[6] ERTZ M, KNOTHE K. A Comparison of analytical and numerical methods for the calculation of temperature in wheel/rail contact[J]. *Wear*, 2002, 253(3–4): 498–508.

[7] FISCHER F D, DAVES W, WERNER E A. On the temperature in the wheel-rail rolling contact[J]. *Fatigue Fract Engng Mater Struct*, 2003, 26(10): 999–1 006.

[8] KENNEDY T C, PLENGSAARD C, HARDER R F. Transient heat partition factor for a sliding railcar wheel[J]. *Wear*, 2006, 261(7–8): 932–936.

[9] ERTZ M, KNOTHE K. Thermal stresses and shakedown in wheel/rail contact[J] *Archive of Applied Mechanics*, 2003, 72(10): 715–729.

[10] FISCHER F D, WERNER E, YAN W Y. Thermal stresses for frictional contact in wheel-rail system[J]. *Wear*, 1997, 211(2): 156–163.

[11] KULKARNI S M, RUBIN C A, HAHN G T. Elasto-plastic coupled temperature-displacement finite element analysis of two-dimensional rolling-sliding contact with a translating heat source[J]. *Journal of Tribology*, 1991, 113(1): 93–101.

[12] WIDIYARTA I M, FRANKLIN F J, KAPOOR A. Modelling thermal effects in ratcheting-led wear and rolling contact fatigue[J]. *Wear*, 2008, 265(9–11): 1 325–1 331.

[13] WU L, WEN Z F, LI W, et al. Thermo-elastic-plastic finite element analysis of wheel/rail sliding contact[C]//*The 8th International Conference on Contact Mechanics and Wear of Rail/Wheel Systems (CM2009)*, Firenze, Italy, September 15–18, 2009, 3: 853–859.

[14] MAKSYM S, KWAN S L, HONG H Y, et al. Numerical calculation of temperature in the wheel-rail flange contact and implications for lubricant choice[J]. *Wear*, 2010, 268(1–2): 287–293.

[15] WEN Z F, JIN X S, JIANG Y Y. Elastic-plastic finite element analysis of nonsteady state partial slip wheel-rail rolling contact[J]. *Journal of Tribology*, 2005, 127(4): 713–721.

[16] JOHNSON K L. *Contact mechanics*[M]. Cambridge: Cambridge University Press, 1985.

[17] CARTER F W. On the action of a locomotive driving wheel[J]. *Proc. R. Soc. London*, 1926, A112: 151–157.

[18] PAUK V, ZASTRAU B. 2D rolling contact problem involving frictional heating[J]. *International Journal of Mechanical Sciences*, 2002, 44(12): 2 573–2 584.

[19] CHEN Y C, KUANG J H, CHEN L W, et al. Wheel-rail thermal contact on rail corrugation during wheel braking[C]//*ASME International Mechanical Engineering Congress and Exposition*, November 5–11, Orlando, Florida USA, 2005: 417–424.

[20] JIN Xuesong, LIU Qiyue. *Tribology between wheel and rail*[M]. Beijing: China Railway Pulishing House Press, 2004. (in Chinese)

[21] BRANDON T, JEFF G, BENJAMIN P A. Investigation of the effects of sliding on wheel tread damage[C]//*Proceeding of ASME International Mechanical Engineering Congress and Exposition (IMECE2005)*, November 5–11, Orlando, Florida USA, 2005: 1–7.

[22] LI Wei, WEN Zefeng, WU Lei, et al. Thermo-elasto-plastic finite element analysis of rail during wheel sliding[J]. *Journal of Mechanical Engineering*, 2010, 46(10): 95–101. (in Chinese)

[23] BAUMANN G, FECHT H J, LIEBELT S. Formation of white-etching layers on rail treads[J]. *Wear*, 1996, 191(1–2): 133–140.

Biographical notes

LI Wei, born in 1985, is currently a PhD candidate at *State Key Laboratory of Traction Power, Southwest Jiaotong University, China*. He received his master degree from *Southwest Jiaotong University, China*, in 2010. His research interests include wheel-rail rolling contact fatigue.
Tel: +86-28-87634480; E-mail: 1022liwei@163.com

WEN Zefeng, born in 1976, is currently a professor and a PhD candidate supervisor at *State Key Laboratory of Traction Power, Southwest Jiaotong University, China.* His main research interests include wheel-rail interaction.
Tel: +86-28-86466051; E-mail: zefengwen@126.com

JIN Xuesong, born in 1956, is currently a professor and a PhD candidate supervisor at *State Key Laboratory of Traction Power, Southwest Jiaotong University, China*. His main research interests include wheel-rail interaction and vehicle-track vibration and noise.
Tel: +86-28-87634355; E-mail: xsjin@home.swjtu.edu.cn

WU Lei, born in 1981, is currently a PhD candidate at *State Key Laboratory of Traction Power, Southwest Jiaotong University, China*. His main research interests include wheel-rail contact damage and vehicle-track dynamics.
E-mail: leiwulanxia@163.com